Pergamon

www.elsevier.com/locate/jaerosci

PII: S0021-8502(99)00058-0

*J. Aerosol Sci.* Vol. 31, No. 3, pp. 307–319, 2000

Printed in Great Britain
0021-8502/00/$ - see front matter

# PHYSICAL AND CHEMICAL (RAMAN) CHARACTERIZATION OF BIOAEROSOLS—POLLEN

M. L. Laucks,* G. Roll,† G. Schweiger† and E. J. Davis*‡

* Department of Chemical Engineering, University of Washington, Seattle, WA 98195-1750, U.S.A.
† Lehrstuhl für Laseranwendungstechnik und Meßsysteme, Maschinenbau, Ruhr-Universität-Bochum, 44780 Bochum, Germany

(*First received* 16 *March* 1999; *and in final form* 16 *April* 1999)

**Abstract**—The chemical characterization of pollen is explored using fluorescence spectroscopy and two Raman spectroscopic techniques. The on-line Raman technique involves trapping single pollen particles in an electrodynamic balance coupled to a Raman spectrometer. The off-line method requires the pollen samples to be deposited on a substrate and analyzed using a Raman microprobe. It is shown that fluorescence spectra of various grass and tree pollens do not show sufficient differences to provide an adequate method for characterizing them. Furthermore, the strong fluorescence masks any underlying Raman spectra. Although photochemical bleaching can reduce the fluorescence signal, it is shown that use of a near-IR laser provides Raman signals that can be used to characterize the pollen particles. In the on-line system, the particle density was determined from electrodynamic springpoint measurements and the geometric pollen size measured with a video microscope. © 2000 Elsevier Science Ltd. All rights reserved

## INTRODUCTION

Conventional methods for the identification of airborne pollen are largely limited to observation of the pollen with optical or scanning electron microscopes and comparison with reference pollens. This paper offers an alternate approach to the characterization of pollen and possibly other bioaerosols by means of Raman measurements that provide chemical rather than morphological information. Recently, Pinnick *et al.* (1998) showed that biological particles such as *escherichia coli* and *bovine serum albumin* can be characterized somewhat by their fluorescence, and they provided a review of the work done to characterize bioaerosols. Since amino acids such as tryptophan are common to many bioaerosols and strongly fluoresce, the fluorescence spectra of various bioaerosols do not differ greatly.

Manoharan *et al.* (1991) pointed out that many biologically important molecules have electronic transitions in the deep UV ($\lambda < 257$ nm, where $\lambda$ is the wavelength of the electromagnetic radiation), and they obtained resonance Raman spectra for fruit, grass and tree pollens using a dye laser pumped with a Nd–YAG laser to obtain deep UV wavelengths. The pollen particles were suspended in water for the measurements. Their results suggest that plant families have distinctly different pollen spectra, for the spectra of fruit pollen (Rosaceae), ragweed (Compositae) and grass (Gramineae) could be clearly distinguished from one another. The grass and ragweed pollens showed evidence of protein tryptophan and tyrosine, but whole fruit pollen showed no detectable peaks associated with aromatic amino acids.

Although resonance Raman offers a promising approach to the chemical characterization of bioaerosols, it is desirable to avoid using aqueous suspensions, for pigments such as flavanoid compounds are water soluble. Flavanoids and flavanols impart the yellow color to many pollens. An alternate approach to the use of aqueous suspensions that remove water soluble material is to electrodynamically trap pollen particles directly from the atmosphere and analyze them by Raman spectroscopy. The use of deep UV is prohibited because the particles must be charged to levitate them in the ac and dc electric fields of the

‡ Author to whom correspondence should be addressed.

electrodynamic balance (EDB), and deep UV causes charge-loss. As we shall show, the use of visible light from an argon-ion laser leads to strong fluorescence that masks the weak spontaneous Raman emission.

The objective of this research was to explore methods of chemically characterizing airborne pollen particles using spontaneous Raman spectroscopy and to determine simultaneously the aerodynamic sizes and densities of the various pollens studied. Of primary interest was a method that can be developed for on-line analysis of airborne matter.

## ON-LINE SPECTROSCOPY

Raman scattering measurements from levitated pollen particles were made in an electrodynamic balance (EDB) chamber coupled to a Raman spectrometer. An overview of the experimental apparatus is depicted in Fig. 1. The double-ring EDB was described in detail by Rassat *et al.* (1993), and a cross section of the device is shown in Fig. 2. Several optical ports on the balance chamber permitted illumination, observation and coupling to a Raman spectrometer. A single pollen particle was trapped and stably levitated by applying ac and dc potentials to the double rings. The ac potential applied to both rings was $\sim 2000$ V peak-to-peak. For a negatively charged particle the upper ring was maintained at a positive dc potential and the lower ring was maintained at the opposite potential. For the Raman studies the levitated particle was illuminated from below using the 514 nm line of a 5 W Coherent Innova-90 Ar-ion laser. The balance chamber was mounted on an $x$–$y$ stage so that the trapped particle could be properly aligned with the laser beam. The nominal maximum power of the 514 nm line was 2 W. The 0.65 mm beam waist from the $TEM_{00}$ Gaussian laser mode was focused to a 125 $\mu$m waist (radius) at the particle by a 500 mm focal length lens. During the experiments, the typical laser intensity was between 2 and 8 MW m$^{-2}$. At these intensities there was sufficient radiation pressure to require adjustment of the dc potential, $V_{dc}$, to balance the net force associated with gravity and the electromagnetic radiation pressure. Thus, the dc potential required for stable levitation satisfies the force balance,

$$-C_0 q \frac{V_{dc}}{z_0} = m_p g - F_{pr}, \tag{1}$$

in which $q$ is the coulombic charge on the particle, $2z_0$ is the distance between the electrodes, $C_0$ is a geometrical constant that accounts for the deviation of the electric field from that

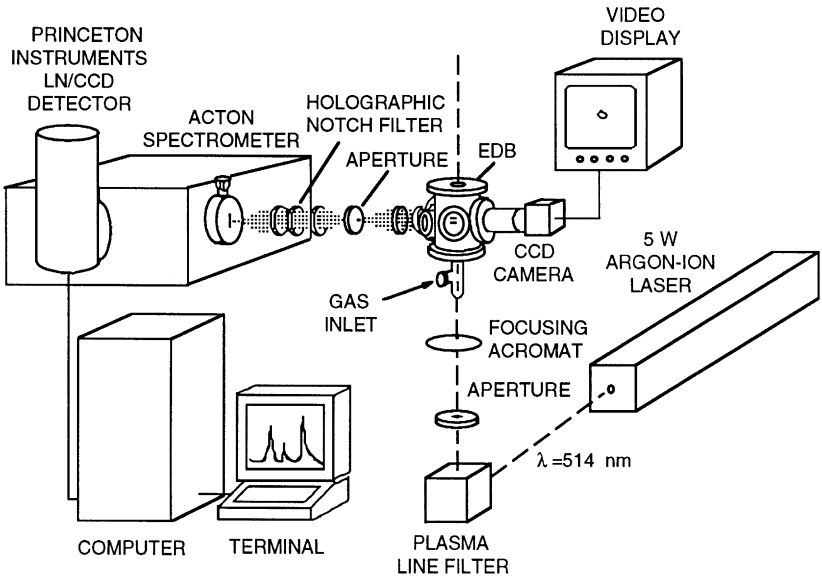


Fig. 1. Overview of the electrodynamic balance system and Raman spectrometer.

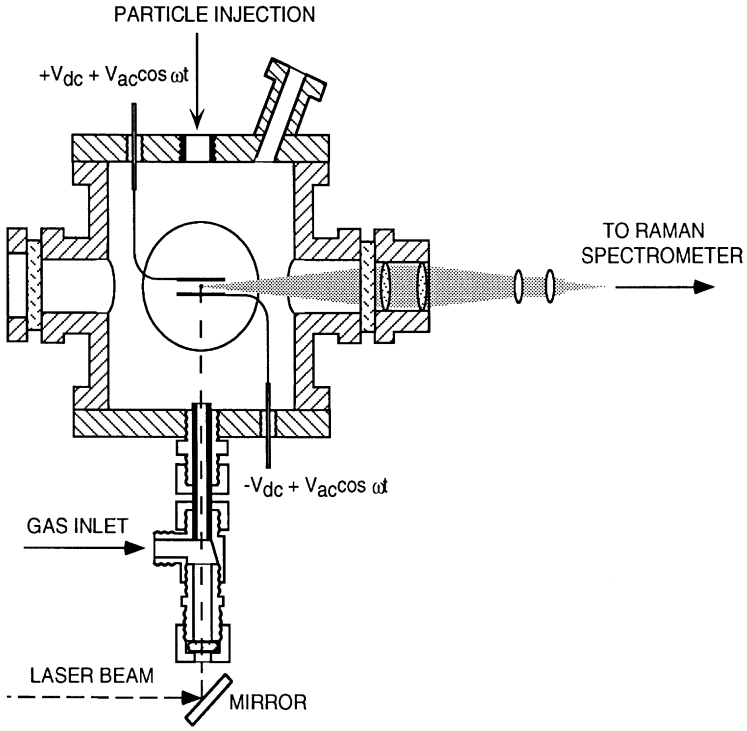


Fig. 2. Cross-sectional view of the electrodynamic balance.

generated by two flat plates of infinite extent, $m_p$ is the particle mass, $g$ is the gravitational constant, and $F_{pr}$ is the radiation pressure force. When there is also gas flow through the chamber the aerodynamic drag exerted by the gas on the particle must be included in the force balance. Dry oxygen could be introduced into the EDB chamber in a steady flow using a control valve and tee attached to the bottom port. In experiments with highly absorbing aerosols a large photophoretic force was encountered due to non-uniform heating of the particle, so the dc potential also had to be adjusted to account for this force.

A video CCD camera with a 7X zoom lens was located outside of one port of the EDB to record the particle image. The effective magnification of zoom lens and video camera was about 400:1. The video system was calibrated using a US Air Force 1951 resolution test chart that could be mounted at the null point of the balance and imaged with the video system. Another port was optically connected to the Raman system. Figure 3 shows the path of the spontaneous Raman signal scattered at 90° to the laser. The signal was outcoupled through a lens ($f = 100$ mm) mounted on that port of the chamber and focused on a spatial filter (to remove the background scattered light in the EDB chamber). Another lens ($f = 40$ mm) collimated the expanding light onto the surface of a holographic notch filter, which removed the 514 nm laser line. A second lens ($f = 150$ mm) re-focused this filtered Raman signal onto the entrance slit of a 500 mm focal length, single-pass ($f/6.5$) (Acton SpectraPro-500i) monochromator. The monochromator had a grating turret so that three different dispersions could be easily obtained: 300, 1200, and 2400 lines $mm^{-1}$, with corresponding resolutions for a 100 mm slit at 514 nm of 24.6, 1.89, and 2.27 $cm^{-1}$. A Princeton Instruments back-illuminated, liquid-nitrogen-cooled, $1340 \times 100$ pixel array CCD camera was attached at the focal plane of the rear slit of the monochromator. The typical operating temperature of this camera was $-90$°C, and integration times between 1 and 60 s were used.

The pollen studied included cottonwood, redwood, paper mulberry, ragweed, sweet vernalgrass (obtained from Bayer), Kentucky bluegrass and grass smuts (from Duke Scientific). Although some of these pollen particles were approximately spherical and were

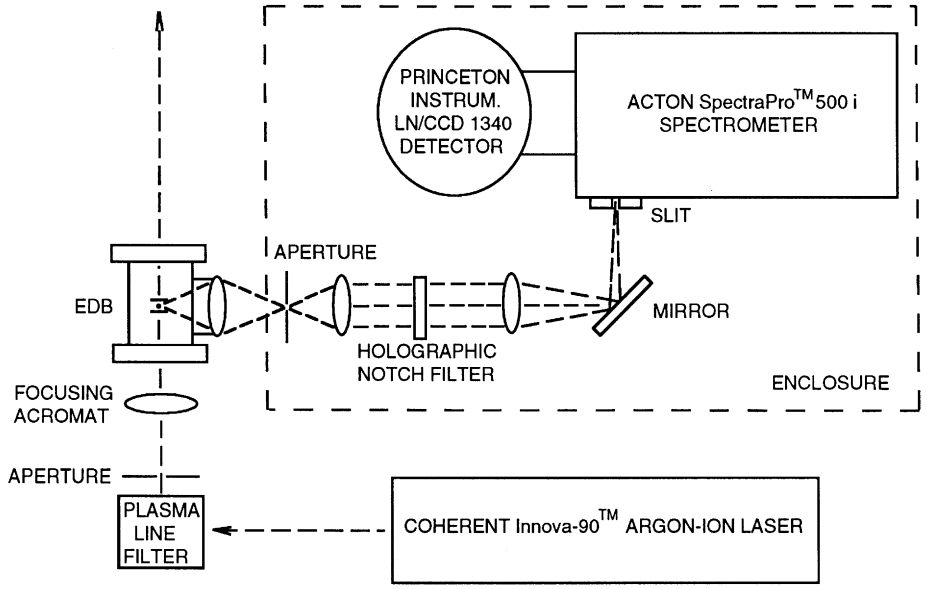


Fig. 3. Raman spectrometer used with the electrodynamic balance.

not strongly absorbent at 514 nm, the dark smuts were highly absorbing at 514 nm. Many of the other non-absorbing pollens were spheroidal. The non-spherical and highly absorbing pollens were sensitive to the photophoretic force of an intense laser beam and were often difficult to trap. Pollen particles were introduced into the EDB on the end of a long insulated hypodermic needle. For some of the pollen studies the needle was touched lightly to the electrode rings, charging the pollen particles due to the instantaneous applied voltage. In other studies, the needle was charged by applying a 3–6 kV square-wave pulse. The ac and dc voltages superposed on the rings were adjusted to stably trap the particle at the center of the chamber. In most cases multiple particles were trapped by this method, and all but one had to be eliminated by destabilizing the other particles. This was accomplished by changing either the ac potential or the frequency to produce oscillations that would cause the undesired particles to collide with the chamber walls or rings thereby being removed. This instability was also used to determine the aerodynamic size and density of the levitated particle as discussed in the following section.

## AERODYNAMIC SIZING AND DETERMINATION OF POLLEN DENSITY

The dynamics of a charged particle in an EDB were analyzed by Frickel *et al.* (1978), and Davis (1985) showed that the stability characteristics of the particle can be used to determine its aerodynamic size. Davis and Periasamy (1985) compared such a method with light scattering data for microspheres, and recently Aardahl *et al.* (1997a, b) and Swanson *et al.* (1999) used stability measurements to determine the aerodynamic sizes of irregularly shaped particles.

The equation of motion for the vertical direction, which is the direction in which the instability occurs, is

$$m_p \ddot{z} = -m_p g - 3\kappa\pi d_p \mu \dot{z} + qC_0 \frac{V_{dc}}{z_0} + qC_1 \frac{V_{ac}}{z_0^2} z \cos \omega t + F_z, \tag{2}$$

in which $\kappa$ is a shape factor that accounts for corrections to Stokes law for non-spherical particles, $\mu$ is the gas viscosity, $d_p$ is the aerodynamic diameter of the particle, $V_{ac}$ is the amplitude of the ac potential, $\omega = 2\pi f$, where $f$ is the ac frequency, and $F_z$ is the sum of

other vertical forces. The geometrical constants, $C_0$ and $C_1$, associated with dc and ac electric fields, respectively, must be determined for the specific geometry of the electrode system.

Equation (2) has a stable, non-oscillatory solution when the dc field balances the gravitational and other external vertical forces, that is, when equation (1) is satisfied with $F_{pr}$ replaced by the sum of the external forces. Then, equation (2) reduces to

$$\ddot{z} + \frac{3\kappa\pi d_p \mu}{m_p}\dot{z} - qC_1\frac{V_{ac}}{m_p z_0^2} z\cos\omega t = 0. \tag{3}$$

The particle position described by this equation is stable at the null point of the chamber provided that the ac potential is not too large. The stability is governed by a dimensionless ac field strength parameter, $\beta$, and a dimensionless drag parameter, $\delta$, defined by

$$\beta = \frac{2qC_1 V_{ac}}{m_p z_0^2 \omega^2} \quad \text{and} \quad \delta = \frac{6\kappa\pi d_p \mu}{m_p \omega}. \tag{4}$$

There exists an infinite set of unstable regions in $\beta$–$\delta$ space, and Müller (1960) obtained an approximate solution for the first marginal stability curve, and the exact solution was determined by Frickel and his coworkers. The marginal stability curve, or set of *springpoints*, separates a region of stability from instability. Starting from a stable state, as either $V_{ac}$ is increased or $\omega$ is decreased, a point is reached at which sudden and violent oscillation occurs. This large-amplitude oscillation can lead to loss of the particle, and the initiation of this oscillation depends on the aerodynamic drag on the particle.

The lowest region of instability is shown in Fig. 4 for Müller's solution and for the exact solution. Müller's equation for the marginal stability state or critical value of $\beta$, above which instability occurs, is

$$\beta_{crit}^2 = \tfrac{1}{2}(99 + 12\delta^2) - \sqrt{\frac{1}{4}(99 + 12\delta^2)^2 - (1 + 4\delta^2)(81 + 36\delta^2)}. \tag{5}$$

The stability results presented in Fig. 4 can be used to determine the aerodynamic size of the levitated particle by measuring $\beta_{crit}$. The determination of $\beta_{crit}$ from measurement of the ac potential and frequency requires knowledge of the balance constants in equation (2). To obtain the desired information we trapped single glass spheres (diameter = 19.9 $\mu$m, $\rho = 2520\ \mathrm{kg\,m^{-3}}$) and measured the springpoints. If a glass particle is trapped with only the

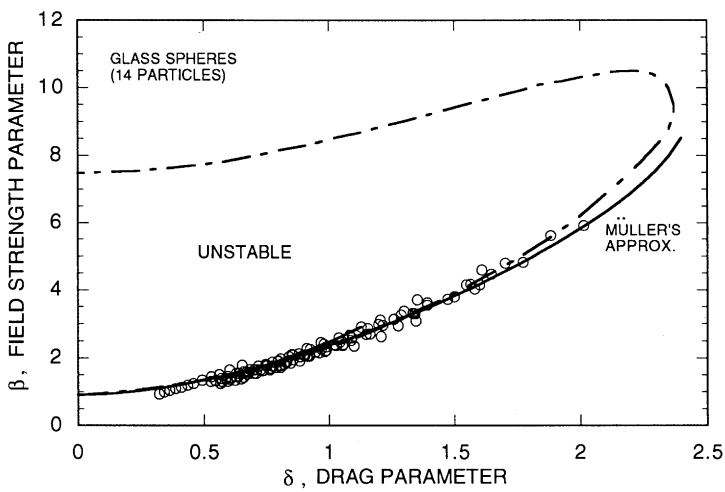


Fig. 4. A particle stability map showing the lowest marginal stability envelope (- - -), Müller's approximation (——), and springpoint data for single glass microspheres.

gravitational force and the dc field acting on the particle, equation (1) with $F_{pr} = 0$ can be re-arranged to

$$\frac{q}{m_p} = -\frac{gz_0}{C_0 V_{dc,0}}. \tag{6}$$

Using this result in the definition of $\beta$, we obtain

$$\beta = \frac{2g}{z_0\omega^2}\left(\frac{C_1}{C_0}\right)\left(\frac{V_{ac}}{V_{dc,0}}\right). \tag{7}$$

Thus, since the only unknowns in $\beta$ and $\delta$ (beside the ratio of constants to be determined) are $f$, $V_{ac}$ and $V_{dc,0}$ ($\kappa = 1$ for spheres), we can measure a set of parameters $f$ and $V_{ac}$ at $V_{dc,0}$ and determine a set of $\beta$ and $\delta$ that can be fit to the marginal stability curve of Fig. 4 using the ratio $C_1/z_0C_0$ as the free parameter. Once this ratio has been determined for the balance, we can determine the density of the pollen particles with this same method, using optical measurements.

Most of the pollen particles analyzed in this study can be approximated as spheres or spheroids. Oberbeck (1876) first examined creeping flow around more general ellipsoids, and Kasper (1982) and Leith (1987) reviewed the work related to drag on non-spherical particles and their size characterization. Kasper showed that the shape factors determined experimentally for oblate and prolate spheroids agreed very well with theory. Oberbeck's solution for the component of force in the $x$-direction for an ellipsoid with principal axes having lengths $2a$, $2b$, $2c$ in the $x$, $y$, $z$ directions, respectively, is

$$F_x = -16\pi\mu abc\frac{v_x}{(\chi_0 + a^2\alpha_0)}, \tag{8}$$

where

$$\chi_0 = abc\int_0^\infty \frac{ds}{\sqrt{(a^2+s)(b^2+s)(c^2+s)}} \tag{9}$$

and

$$\alpha_0 = abc\int_0^\infty \frac{ds}{(a^2+s)\sqrt{(a^2+s)(b^2+s)(c^2+s)}}. \tag{10}$$

The shape factor for an ellipsoid that has the same drag force as a sphere with radius $R$ is

$$\kappa = \frac{8}{3}\frac{abc}{R(\chi_0 + a^2\alpha_0)}. \tag{11}$$

Substituting this value into the expression for $\delta$ in equation (4) and using $d_p = 2R$ (the aerodynamic size of the ellipsoid), the dimensionless drag parameter for an ellipsoid is

$$\delta = \frac{32\pi\mu abc}{m\omega(\chi_0 + a^2\alpha_0)}. \tag{12}$$

In our experiments, the majority of spheroidal pollen particles were oriented in the EDB as prolate spheroids with the minor axis in the vertical direction. When oscillating, their motion was in the direction normal to the major axis. For an prolate spheroid with minor semi-axes $a = c$ and major semi-axis $b$, the volume is $4\pi a^2 b/3$, the mass is $m = 4\pi a^2 b\rho/3$, and the aerodynamic size is

$$2R = 2\sqrt[3]{a^2 b}. \tag{13}$$

In this case the drag parameter becomes

$$\delta = \frac{12\mu}{\rho\pi f(\chi_0 + a^2\alpha_0)}, \tag{14}$$

and the integrals $\chi_0$ and $\alpha_0$ are

$$\chi_0 = \frac{a^2 b}{\sqrt{b^2 - a^2}} \ln\left[\frac{b + \sqrt{b^2 - a^2}}{b - \sqrt{b^2 - a^2}}\right], \tag{15}$$

$$\alpha_0 = \frac{1}{b^2 - a^2}\left[b^2 - \frac{\chi_0}{2}\right]. \tag{16}$$

Occasionally, the spheroids would re-orient with the major axis in the vertical direction. In this case, for a prolate spheroid (with major semi-axis $a$ and minor semi-axes $b = c$), $\delta$ is given by equation (14), but the integrals $\alpha_0$ and $\chi_0$ are

$$\chi_0 = \frac{ab^2}{\sqrt{a^2 - b^2}} \ln\left[\frac{a + \sqrt{a^2 - b^2}}{a - \sqrt{a^2 - b^2}}\right], \tag{17}$$

$$\alpha_0 = \frac{1}{a^2 - b^2}[\chi_0 - 2b^2]. \tag{18}$$

Measurements of the minor and major axes of a pollen grain by means of a video camera permitted us to calculate the integrals $\alpha_0$ and $\chi_0$. With the particle balanced at $V_{dc}$, we determined the values of $\beta$ and $\delta$ corresponding to the transition from stability to instability from measurements of $V_{ac}$ and $f$. We then fit these data points to the Müller approximation equation (5), using the pollen density as the free parameter.

This procedure was carried out for most of the pollen particles studied, and a representative sample of the results is shown in Fig. 5 for a series of 10 measurements of redwood pollen. The data, which fall on the marginal stability curve, are consistent with an average density of 2240 with a standard deviation of 300 kg m$^{-3}$. Table 1 summarizes the measured sizes and densities (determined from springpoint measurements) of the pollen studied. As can be seen in the table, both Kentucky bluegrass and cypress pollen have relatively large standard deviations compared to their average density (29% and 21%, respectively). These pollen particles also had more variation in morphology as seen in the video microscopy images. Although all of the pollen was generally spheroidal, some particles had sharp edges, which may cause errors when applying the spheroidal model. The large standard deviations in Table 1 may be due to both actual density differences between pollen caused by physical differences (e.g., humidity effects—uptake or release of water by the pollen or physical mutations) and errors in applying the spheroidal model to not-perfectly spheroidal particles.

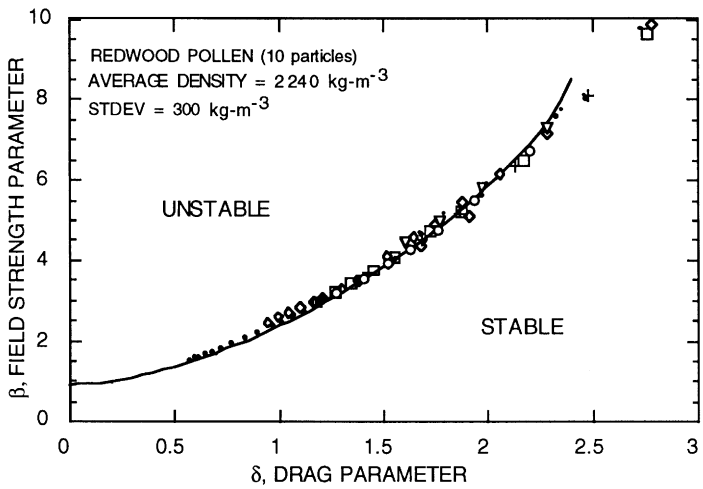


Fig. 5. Marginal stability data for redwood pollen compared to Müller's approximation.

Table 1. Average values for the major and minor axes, aerodynamic sizes ($2R$), and densities of five types of pollen (10 individual particles were measured for each type)

| Pollen type | Dimensions ($\mu$m) | | | | Aero. Size ($\mu$m) | | Density (kg m$^{-3}$) | |
|---|---|---|---|---|---|---|---|---|
| | Minor axis | S.d. | Major axis | S.d. | $2R$ | S.d. | Average | S.d. |
| Sweet vernalgrass | 40 | 6 | 50 | 5 | 42 | 3.0 | 1210 | 200 |
| Kentucky bluegrass | 33 | 4 | 41 | 4 | 35 | 3.5 | 968 | 300 |
| Redwood | 26 | 2 | 42 | 4 | 31 | 1.9 | 2238 | 300 |
| Cypress | 30 | 8 | 34 | 2 | 31 | 3.5 | 1456 | 300 |
| Cottonwood | 27 | 3 | 32 | 4 | 29 | 2.0 | 1744 | 200 |

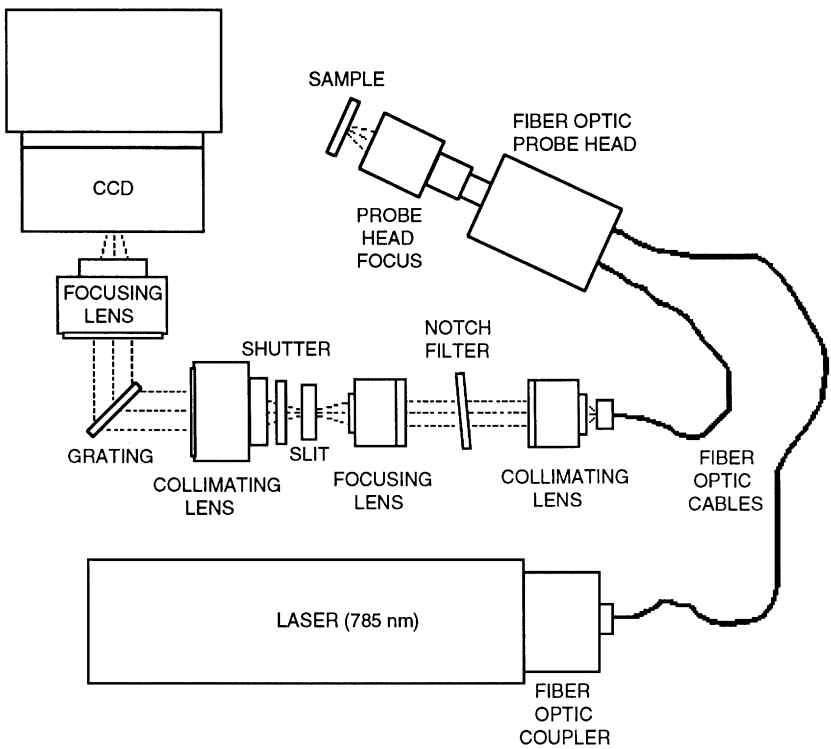


Fig. 6. The Raman microscope system used for near IR measurements.

## OFF-LINE SPECTROSCOPY

Off-line Raman spectral measurements were made using a Kaiser optical systems Raman microscope.* In this system, which is shown in Fig. 6, a high power (250 mW) external cavity wavelength-stabilized laser diode at 785 nm provided light that scattered off a sample placed at the focal point of a confocal microscope. Scattered light was collected by the microscope objective and coupled into fiber optic cables. After being outcoupled from the fiber the signal was collimated and then passed through a Kaiser Holographic Super-Notch Plus filter, which removed the 785 nm laser line. The signal was re-focused onto the slit of a $f/1.8$ spectrometer, dispersed by a grating, and recorded by a back-illuminated NIR thermoelectrically cooled CCD camera. Due to losses in the optical system, the laser power

*The use of the Kaiser Raman microscope was made possible by Dr. Lloyd Burgess at the Center for Process Analytical Chemistry (CPAC) at the University of Washington.

at the sample was approximately 90 mW and the spot diameter was between 5 and 10 $\mu$m, giving an intensity of between 1 and 5 GW m$^{-2}$ at the sample.

A thin layer of pollen was placed on an aluminum microscope slide and the sample was scanned visually through the microscope (in white light) to select an isolated particle for study at 785 nm. Once the microscope was focused on a particle, the white light was switched off and the 785 nm laser was turned on. The Raman spectrum was recorded and displayed with HoloGRAMS and GRAMS software.

## SPECTROSCOPY RESULTS

### *EDB Raman data* (*at 514 nm*)

Figure 7 shows the effect of the presence of $O_2$ gas on the spectrum of sweet vernalgrass. The nitrogen line at 2330 cm$^{-1}$ does not appear in the lower spectrum, which was obtained with oxygen flow through the chamber, and the oxygen line at 1550 cm$^{-1}$ is enhanced.

Note that the broad fluorescence background is substantially decreased by oxygen bleaching, and more Raman structure is revealed. The prominent peak at 2920 cm$^{-1}$ is associated with C–H bonds, and other bonds can be identified in the bleached spectrum. All of the pollens examined exhibited strong fluorescence that masked the Raman signal, but some of the Raman spectrum could be detected after either oxygen bleaching or photobleaching (at 514 nm). In all cases the pollen were bleached until changes in the spectra were minimized. Some pollen was much more sensitive to photophoretic forces (less spherical), so the laser intensity used varied from pollen to pollen. Also the requisite time varied: some pollen bleached almost immediately (cottonwood), while other pollen required bleaching overnight. It does not appear that oxygen alone can achieve adequate bleaching, but oxygen together with photobleaching is partially effective. Barnes *et al.* (1994) observed photobleaching within 1 min in their studies of electrodynamically levitated microdroplets.

Some differences among the various pollens appear in the fluorescence spectra as well as in the Raman spectra. The spectra in Fig. 8 were taken shortly after each pollen particle was trapped in the EDB and prior to photobleaching, and they show the differences in fluorescence spectra among the ragweed, cottonwood, Johnson grass and sweet vernalgrass pollens. Some Raman peaks can also be seen near 1500 and 2900 cm$^{-1}$. Figure 9 presents the results when the same pollens were partially photobleached. The major differences are in the wave number region below 2000 cm$^{-1}$.

While we found that there are some differences in spectra among the pollen studied, we were not able to bleach the pollen sufficiently to obtain distinctive "signature" spectra. In an

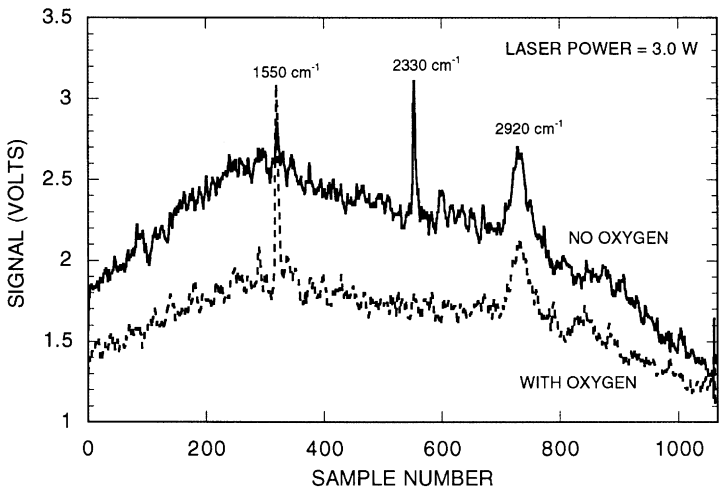


Fig. 7. The effect of oxygen bleaching on the spectrum of sweet vernalgrass pollen.

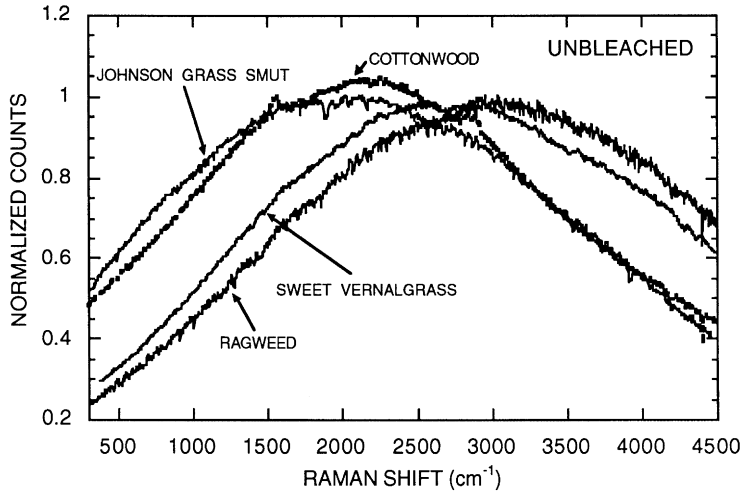


Fig. 8. Fluorescence spectra for Johnson grass smut, sweet vernal grass, cottonwood and ragweed pollen.

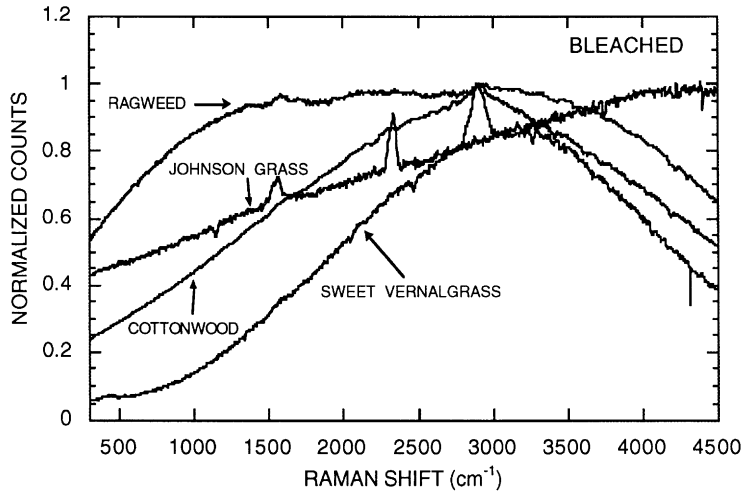


Fig. 9. Partially bleached spectra for Johnson grass smut, sweet vernal grass, cottonwood and ragweed pollen.

attempt to verify that the peaks we saw were Raman peaks and not part of the fluorescence spectrum, we used a Raman microscope spectrograph operating at 785 nm. We discovered that the fluorescence was significantly reduced using the system discussed in the following section.

*Raman microscope spectra* (*at 785 nm*)

In an effort to understand any optical differences between the spectra obtained with EDB Raman spectroscopy system and the Raman microscope spectra, we compared spectra obtained for Polystyrene divinylbenzene (DVB) microspheres using the two systems. The results, shown in Fig. 10, indicate that there is a small offset in Raman shift ($cm^{-1}$) between the two systems. This is most likely due to wavelength calibration errors in one or both systems and amounts to an error of about 7% in the absolute value of the Raman shift. The spectrum from the particle suspended in the EDB is less well-resolved because the spectral resolution was about 25 $cm^{-1}$, whereas the Raman microscope system had a resolution of

4 $cm^{-1}$. But the qualitative aspects of the two spectra (the shape and relative positions of the lines) show very good agreement. Note the presence of the $N_2$ line (at 2350 $cm^{-1}$) in the spectrum for a levitated particle.

The pollen examined in the Raman microscope included all of the pollen explored in the EDB studies except for Johnson grass smut spores. The intensity of the 785 nm laser beam at the sample was sufficient to vaporize the dark smut spores, and it was not possible to take a Raman spectrum for such strongly absorbing species.

Figure 11 shows the spectra of the same pollen as in Figs 8 and 9 (with the exception of the Johnson grass smut spores) taken with the 785 nm Raman microscope. It is clear that there is much less fluorescence background, but the peaks at 2900 and 1600 $cm^{-1}$ are still present, indicating that these are indeed Raman peaks. Because of decreased fluorescence background, there is also much more structure visible in the range of 400–1600 $cm^{-1}$; in fact it is only in this region that the spectra can be distinguished.

Figure 12 is a plot of the spectra for cypress, redwood, paper mulberry, and Kentucky bluegrass pollen. Among the pollen studied, cottonwood, cypress and redwood all had

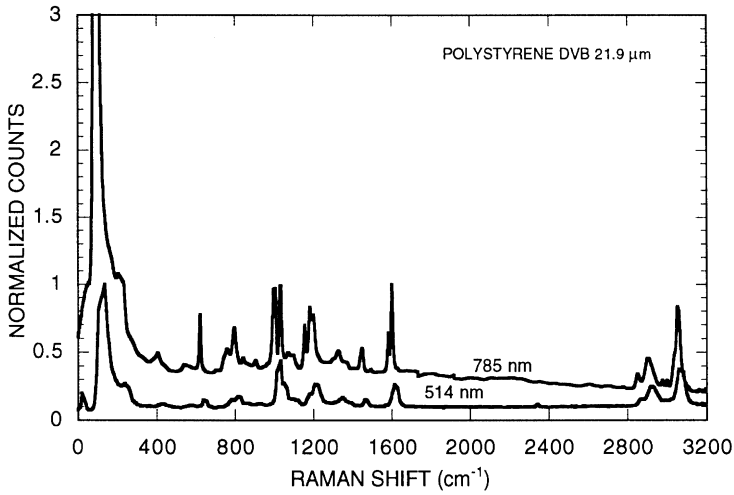


Fig. 10. Raman spectrum for polystyrene di-vinylbenzene microspheres obtained for levitated particles (514 nm laser source) compared with the spectrum obtained with the near IR Raman microscope (785 nm).

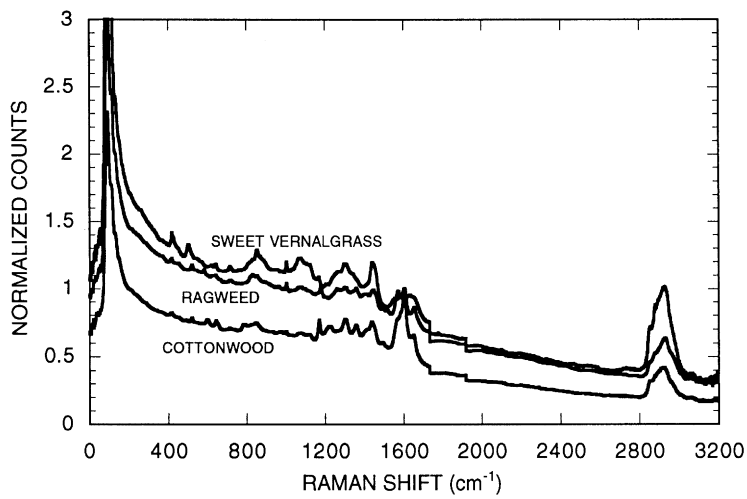


Fig. 11. Raman spectra of sweet vernalgrass, ragweed and cottonwood pollen obtained with the Raman microscope system.

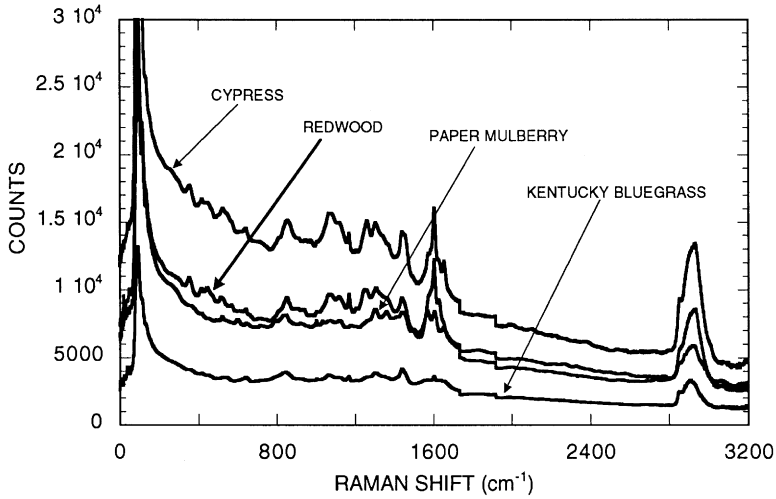


Fig. 12. Raman spectra of cypress, redwood, paper mulberry, and Kentucky bluegrass pollen obtained with the Raman microscope system.

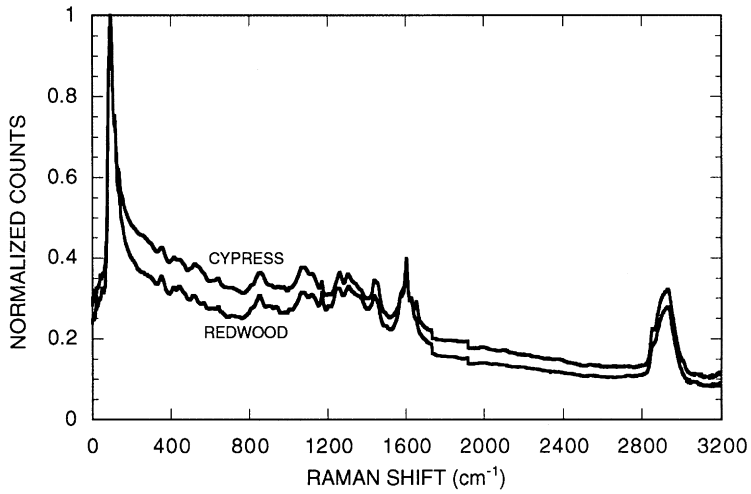


Fig. 13. Raman spectra of cypress and redwood pollen obtained with the Raman microscope system.

a distinct line at 1600 $cm^{-1}$, whereas paper mulberry, ragweed, Kentucky bluegrass, and sweet vernalgrass did not. All the pollen studied showed the 2900 $cm^{-1}$ line characteristic of the C–H bond. In Fig. 13 the spectra of cypress and redwood are compared, and it can be seen that, qualitatively, the two spectra are very similar. It is interesting that cypress (*Cupressus arizonica*) and redwood (*Sequoia sempervirens*,) are both Gymnosperms (class Coniferinae) in the closely related families Cupressaceae and Taxodiaceae, respectively, so it is to be expected that their spectra are similar.

## CONCLUSIONS

We have found that pollens are easily charged and trapped by the EDB. It appears feasible to trap particles from the atmosphere provided that an appropriate charging method is developed, as well as a reliable method of removing multiple trapped particles. Aardahl *et al.* (1997b) examined a variety of methods for charging ambient microparticles

and our experience in trapping many different kinds of particles provides insight into possible algorithms for removing unwanted particles.

Many pollens fluoresce strongly using incident illumination at 514 nm. While some Raman peaks are visible above the background, there were not enough characteristic features to distinguish between the spectra of the different pollen examined. However, we found that by using a 785 nm laser with three orders of magnitude more intensity at the pollen sample, we were able to reduce the fluorescence background to the point where we could distinguish among different pollen "signatures" in the 400–1600 $cm^{-1}$ region of the Raman spectrum.

The use of a 785 nm high-power single-mode diode laser combined with a suitable method of charging pollen particles collected from the atmosphere would allow "on-line" analysis of pollen particles.

*Acknowledgements*—The authors are grateful to the National Science Foundation for Grants CTS-9528897 and INT-9725216 and to the Deutscher Akademischer Austausdienst for the support of this research. We would also like to acknowledge the assistance of Brian Marquadt in obtaining the off-line spectral measurements and to thank Dr Lloyd Burgess for making possible the use of the Kaiser Raman Microscope at the Center for Process Analytical Chemistry, University of Washington.

## REFERENCES

Aardahl, C. L., Vehring, R., Davis, E. J., Schweiger, G. and Swanson, B. D. (1997a) Trapping two-particle arrays in a double-ring electrodynamic balance. *J. Aerosol Sci.* **28,** 1491–1505.

Aardahl, C. L., Vehring, R., Weber, R., Schweiger, G., Davis, E. J. and Wiedensohler, A. (1997b) Electrodynamic trapping of aerocolloidal particles: experimental and theoretical trapping limits. *J. Colloid Interface Sci.* **192,** 228–237.

Barnes, M. D., Whitten, W. B. and Ramsey, J. M. (1994) Enhanced fluorescence yields through cavity quantum-electrodynamic effects in microdroplets. *J. Opt. Soc. Am. B* **11,** 1297–1304.

Davis, E. J. (1985) Electrodynamic balance stability characteristics and applications to the study of aerocolloidal particles. *Langmuir* **1,** 379–387.

Davis, E. J. and Periasamy, R. (1985) Light scattering and aerodynamic size measurements for homogeneous and inhomogeneous microspheres. *Langmuir* **1,** 373–379.

Frickel, R. H., Shaffer, R. E. and Stamatoff, J. B. (1978) Report No. ARCSL-TR-77041, Chemical Systems Laboratory, Aberdeen Proving Ground, MD.

Kasper, G. (1982) Dynamics and measurement of smokes. 1. Size characterization of non-spherical particles. *Aerosol Sci. Technol.* **1,** 187–199.

Leith, D. (1987) Drag on non-spherical objects. *Aerosol Sci. Technol.* **6,** 153–161.

Manoharan, R., Ghiamati, E., Britton, K. A., Nelson, W. H. and Sperry, J. F. (1991) Resonance Raman spectra of aqueous pollen suspensions with 222.5–242.4-nm pulsed laser excitation. *Appl. Spectrosc.* **45,** 307–311.

Müller, A. (1960) Theoretische untersuchungen über das verhalten geladener teilchen in sattelpunkten electrischer wechselfelder. *Ann. Phys.* **6,** 206–220.

Oberbeck, A. (1876) On stationary fluid motions when viscosity is taken into consideration. *J. Math.* **81,** 62.

Pinnick, R. G., Hill, S. C., Nachman, P., Videen, G., Chen, G. and Chang, R. K. (1998) Aerosol fluorescence spectrum analyzer for rapid measurement of single micrometer-sized airborne biological particles. *Aerosol Sci. Technol.* **28,** 95–104.

Swanson, B. D., Bacon, N. J., Davis, E. J. and Baker, M. B. (1999) Electrodynamic trapping and manipulation of ice crystals. *Q. J. R. Meteorol. Soc.* **125,** 1039–1058.